J Mater Sci (2007) 42:1673–1681
DOI 10.1007/s10853-006-0909-7

Microstructure and mechanical properties of commercial purity titanium severely deformed by ARB process

Daisuke Terada · Seiya Inoue · Nobuhiro Tsuji

Received: 27 June 2006 / Accepted: 31 August 2006 / Published online: 13 January 2007

Abstract Commercial purity titanium was deformed by accumulative roll-bonding (ARB) process up to 8 cycles (equivalent strain of 6.4) at ambient temperature. This is the first study on ultra-high straining of h.c.p. metals by the ARB process. The microstructure of the ARB-processed specimens showed two kinds of characteristic ultrafine microstructures. One was the lamellar boundary structure elongated along RD, which has been also reported in the ARB-processed cubic metals. The lamellar boundary spacing decreased with increasing ARB strain and reached about 80 nm after 5 ARB cycles. The other microstructure was the equiaxed grains having mean grain size of 80–100 nm. Such a fine and equiaxed grain structure has not yet been reported in the as-ARB-processed materials before. The fraction of the equiaxed grains increased as the ARB process proceeded, and 90% of the specimen was filled with the equiaxed grains after 8 ARB cycles. As the number of the ARB process increased, the tensile strength increased and the total elongation decreased gradually. After 6 ARB cycles, the specimen exhibited almost the same mechanical properties as that of commercial Ti-6Al-4V alloy.

Introduction

It has been already established that severe plastic deformation (SPD) can realize the ultrafine grained (UFG) or sometimes nanocrystalline (NC) microstructures in metallic materials [1–5]. The formation mechanism of the UFG/NC microstructure has been an issue of argument, and many researchers have studied the microstructure evolution during SPD. One of the ideas to explain the microstructure evolution during SPD is grain subdivision [6, 7]. The grain subdivision [8] is a process where deformation induced boundaries subdivide the original crystals. The deformation induced boundaries are categorized into two types: incidental dislocation boundaries (IDBs) and geometrically necessary boundaries (GNBs) [8]. In the ultrahigh strained materials, a number of GNBs are introduced to form the UFG microstructures. The grain subdivision has been systematically studied in f.c.c. metals and alloys in which slip systems can be strictly determined.

On the other hand, the SPD processes have been applied mainly to metals and alloys having cubic crystal structure, and the number of SPD studies on hexagonal materials is limited. It is well known that deformation behaviors of hexagonal metals are significantly different from those of cubic metals. Number of active slip systems is limited, and sometimes deformation twining plays an important role for plastic deformation [9]. Thus, it is expected that the microstructure evolution during SPD is different between cubic and hexagonal metals. The purpose of the present study is to clarify the change in microstructures and mechanical properties in pure titanium (Ti) during SPD. Ti is a typical h.c.p. metal. Pure Ti is also important for various kinds of practical applications, because of its lightness, strength, formability, and biological harmlessness. If pure Ti can be strengthened by grain refinement, the applicability of this metal would be further widened. SPD of pure Ti has been conducted by high pressure

D. Terada (✉) · S. Inoue · N. Tsuji
Department of Adaptive Machine Systems,
Graduate School of Engineering, Osaka University, Osaka, Japan
e-mail: terada@ams.eng.osaka-u.ac.jp

torsion (HPT) at room temperature (RT) [10], by multiple forging at 400–550 °C or RT [11], by equal channel angular pressing (ECAP) at 450–500 °C and subsequent HPT at RT [12], by HPT at RT [13], by ECAP of route-B at 400–450 °C [14], by ECAP of route-Bc at 350–450 °C followed by conventional cold rolling [15, 16], by *abc*-forging at 400 °C [17] and by repeated cold-rolling [18]. These studies showed UFG microstructures after SPD, but the microstructure evolution during SPD is still unclear due to lack of systematic observations.

In the present study, a commercial purity Ti (CP-Ti) is severely deformed by the accumulative roll bonding (ARB) process. Figure 1 illustrates the principle of the ARB process. The ARB is an SPD process using rolling deformation [19–22], and it is applicable to continuous production of sheet materials. The ARB has been applied to various kinds of metals and alloys and UFG microstructures were successfully obtained [19–22]. However, the ARB has been used only for cubic materials and this is the first trial to apply the ARB to h.c.p. metal.

Experimental

A CP-Ti (ASTM grade 2) sheets 2 mm in thickness, 40 mm in width and 200 mm in length were used in this study. The starting sheet had equiaxed grains with the mean grain size of 10 μm. The chemical composition of the material is shown in Table 1. The starting sheets were firstly deformed to 50% reduction in thickness (equivalent strain of 0.8) by conventional rolling at RT. This procedure is hereafter considered as the first ARB cycle. The 50% cold-rolled sheets 1 mm thick were cut in half-length, stacked to be 2 mm thick after degreasing and wire-brushing the contact surfaces, and then roll-bonded by 50% reduction in one pass at RT, which is considered as the second ARB cycle. The procedures in the second ARB cycle were repeated up to 8 ARB cycles (total equivalent strain of 6.4). The ARB was carried out under well-lubricated condition using a two-high mill having a roll diameter of 310 mm. The roll peripheral speed was 0.29 m s^{-1}, so that the mean strain rate during rolling was 19 s^{-1}. The sheets were cooled into water immediately after roll-bonding.

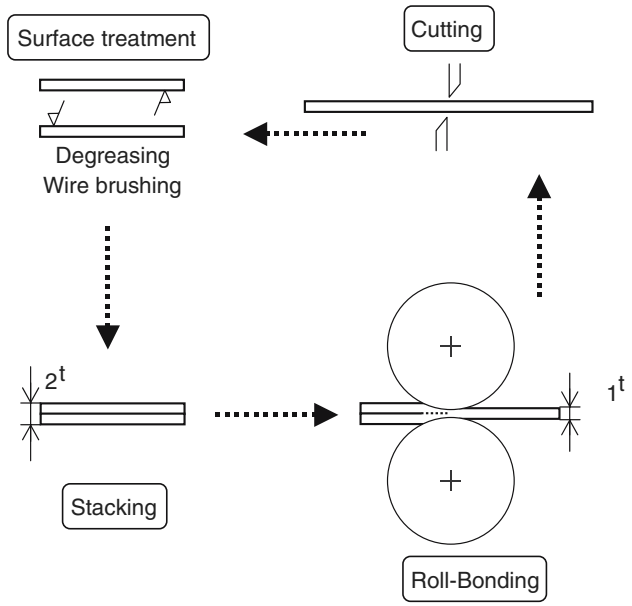

Fig. 1 Schematic illustration showing the principle of the accumulative roll-bonding process

The microstructure characterizations of the CP-Ti sheets ARB-processed by various cycles (various strains) were carried out by scanning electron microscopy (SEM) and transmission electron microscopy (TEM). The observed sections for SEM were perpendicular to the transverse direction (TD) of the sheets. The observed plane was electro-polished in 50 ml $HClO_4$ + 350 ml $CH_3(CH_2)_2CH_2OH$ + 600 ml CH_3OH solution and then etched with a 10 ml HF + 40 ml HNO_3 + 50 ml H_2O solution. Phillips XL30S SEM equipped with field-emission (FE) type gun was operated at 15 kV. Orientation analysis was also carried out by electron back-scattering pattern (EBSP) analysis in the same FE-SEM. TSL-OIM software was used for EBSP measurement and analysis. For TEM observations, thin foils perpendicular to TD were prepared by twin-jet electro-polishing in the same solution described above. TEM observations were carried out by the use of Hitachi H-800 operated at 200 kV.

Tensile tests were conducted for the ARB-processed specimens at RT. Tensile specimens 5 mm in gage width and 10 mm in gage length (1/5 of JIS-5 specimen) were tested at initial strain rate of 8.3×10^{-4} s^{-1}. The tensile direction was parallel to the rolling direction (RD) of the sheets.

Results

Microstructure of ARB specimens

Figure 2 shows SEM microstructures of the CP-Ti specimen before the ARB (a) and those ARB-processed by various cycles (b–f). The starting material (Fig. 2a) had equiaxed grains with mean grain size of 10 μm. The specimen ARB-processed by 1 cycle (50%

Table 1 Chemical composition of the commercial purity titanium (wt.%)

C	H	O	N	Fe	Ti
0.007	0.0013	0.08	0.004	0.05	Bal.

rolled) (a) and 2 cycles (b) showed elongated initial grains involving complicated deformation microstructures inside. After 4 cycles, very fine and elongated structures were observed (d–f). The arrows in Fig. 2 indicate the shear bands and are parallel to the shear band direction. Shear bands penetrating many initial grains also appeared after 2 ARB cycles. The shear bands had various tilt angles to RD ranging from a few degrees to about 30°. However, newly introduced (fresh) shear bands seemed to have 30° title angle, and probably the shear bands appeared in the former cycles fell down to smaller angles with increasing the total reduction. Width of each shear bands varied from 0.2 to 1.2 μm.

Figure 3 shows area fraction of the shear bands measured from the SEM microstructures of the CP-Ti ARB-processed by various cycles. Here, ''fresh shear bands'' (solid circle) are defined as the bands titled by 30° to RD. Because it was difficult to distinguish the shear bands having very small tilt angles from the matrix elongated to RD, the area fraction of ''observed shear bands'' (open circle) does not include the shear bands with tilt angles smaller than 10°. ''Cumulative shear bands'' (open triangle) in Fig. 3 means the cumulative values of the ''fresh shear bands''. The area fraction of the fresh shear bands showed nearly constant values of 2–4% after each cycle, though it slightly increased with increasing the number of ARB cycle. After 6 ARB cycles, the area fraction of fresh shear bands obviously decreased as the deformation proceeds. The observed shear bands increased with increasing strain and showed nearly constant value of 8% after the sixth cycle. The area fraction of the cumulative shear bands monotonously increased as the number of ARB cycle increased, and reached to 23% after 8 ARB cycles.

In order to clarify the more detailed deformation microstructures, TEM observation was conducted to the ARB-processed samples. TEM microstructures of the CP-Ti ARB-processed by 2 cycles are shown in Fig. 4. The microstructures were basically complicated dislocation cell structures with high dislocation density. The shear bands observed in SEM were also recognized in TEM microstructures (Fig. 4a–c). Some of the shear bands were composed of fine and elongated structure parallel to the longitudinal direction of the bands, while some exhibited very fine and nearly equiaxed substructures (Fig. 4d). The mean interval of the lamellar boundaries in Fig. 4b and the mean diameter of the nearly equiaxed grains in Fig. 4d were 370 and 120 nm, respectively. Figure 5 shows TEM microstructures of the CP-Ti ARB-processed by 4 cycles. Most of the area showed lamellar structure

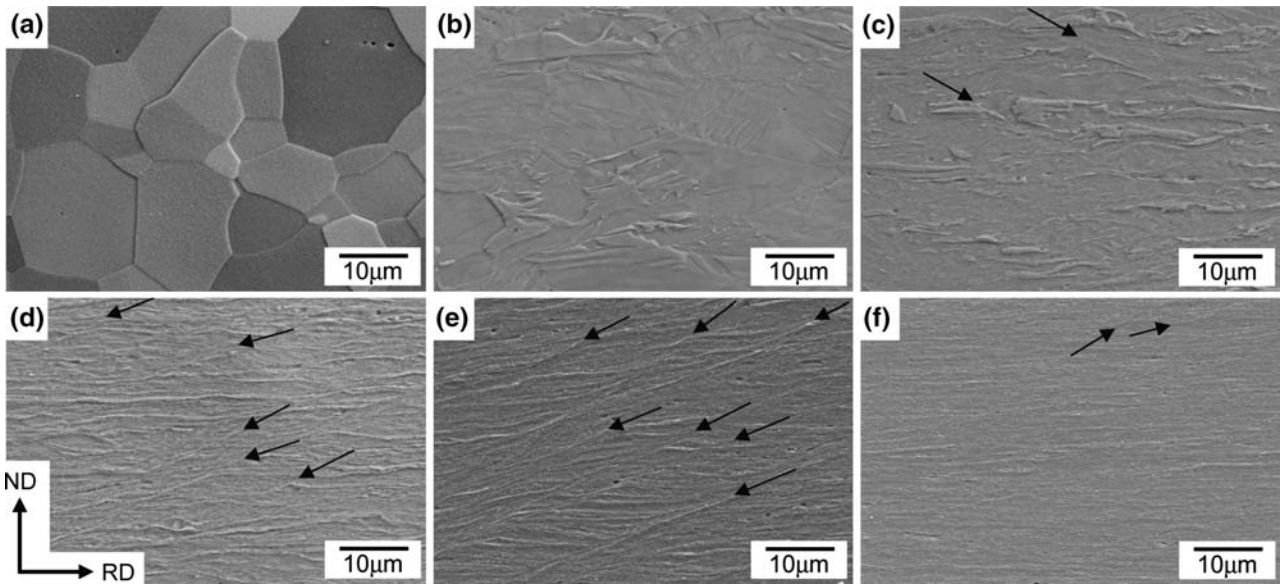

Fig. 2 SEM microstructures on longitudinal sections of the commercial purity Ti (**a**) before ARB and ARB-processed by (**b**) 1 cycle, (**c**) 2 cycles, (**d**) 4 cycles, (**e**) 6 cycles and (**f**) 8 cycles at room temperature. The *arrows* indicate shear bands and are parallel to the direction of each shear band

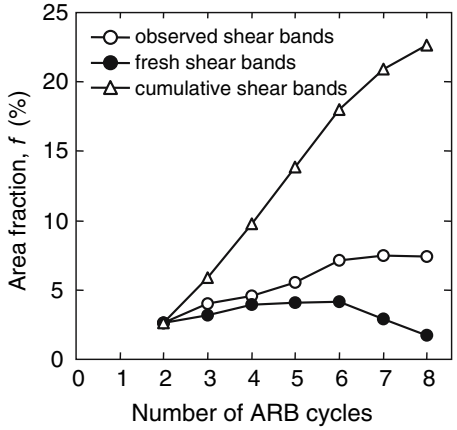

Fig. 3 Area fraction of the shear bands in the commercial purity Ti ARB-processed by various cycles at room temperature

elongated to RD. The interval of the lamellar boundaries varied from several tens nanometer to several hundreds nanometer, and the mean interval was 140 nm. Typical lamellar boundary structure is shown in Fig. 5b, which is quite similar to the ultrafine lamellar boundary structures observed in the cubic metals ARB-processed [17–22]. In the 4-ARB cycled specimen, equiaxed grains were also observed in part. Figure 5c shows a typical example of the equiaxed grains. The mean grain size was 100 nm. Such fine and equiaxed grains have not yet been observed in the as-ARB-processed cubic materials. The selected area diffraction (SAD) patterns of the lamellar boundaries and the equiaxed grains (Fig. 5b, c) showed complicated or ring-like patterns, which indicated the both microstructures involved large local misorientations. Figure 6 shows TEM microstructures of the specimens ARB-processed by 6 cycles (a) and 8 cycles (b). In the 6-cycle specimen, both lamellar boundary structure with mean boundary interval of 70 nm and the equiaxed grain structure having mean grain size of 90 nm were seen (Fig. 6a). In the 8-cycle specimen (Fig. 6b), the microstructure was mostly filled with the equiaxed grains. The mean grain size of the equiaxed grains and the mean interval of the lamellar boundaries partly observed were both 80 nm.

It was clarified in the TEM observations that two kinds of characteristic ultrafine microstructures, i.e., lamellar boundary structure and equiaxed grain structure, were formed in the CP-Ti highly deformed by the ARB process. It should be emphasized that the equiaxed grain structure has not yet been observed in the as-ARB-processed specimens before. It should be also noted that the present ARB process of the CP-Ti was conducted at RT, where recovery and recrystallization were hard to occur. Area fractions of the lamellar boundary structure, the equiaxed grain structure and other microstructures were evaluated from the TEM micrographs, and the obtained results are shown in Fig. 7. The ''other microstructures'' correspond to the complicated dislocation cells observed in Fig. 4, for example, that are neither lamellar boundary structure nor equiaxed grain structure. The area fraction of the lamellar boundary structure firstly increased with increasing the number of ARB cycle,

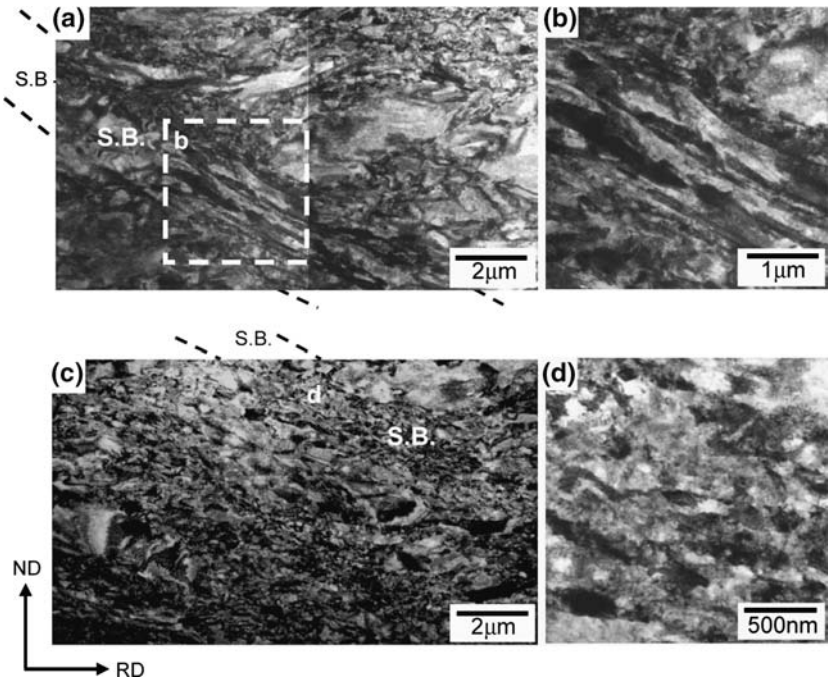

Fig. 4 TEM microstructures of the commercial purity Ti ARB-processed by 2 cycles at room temperature. (**b**), (**d**) High magnification micrographs of the shear bands in (**a**) and (**c**), respectively

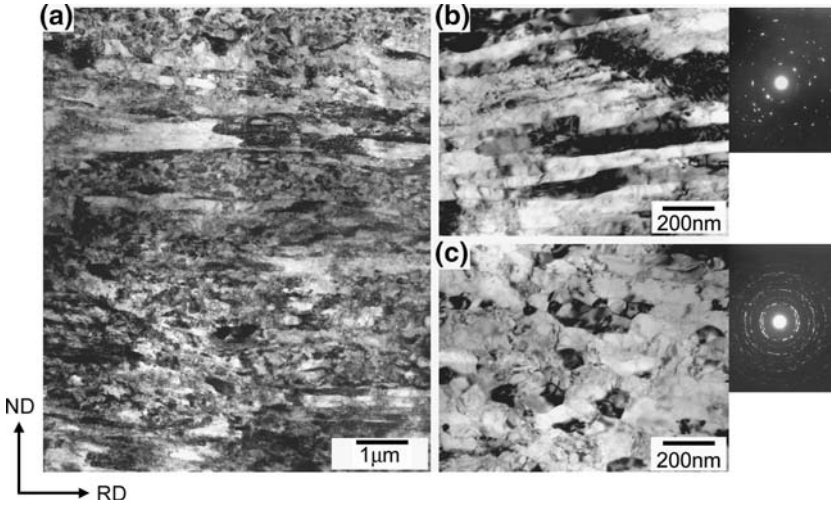

Fig. 5 TEM microstructures of the commercial purity Ti ARB-processed by 4 cycles at room temperature (**a**). (**b**), (**c**) High magnification micrographs of the lamella structure and equiaxed structure, respectively

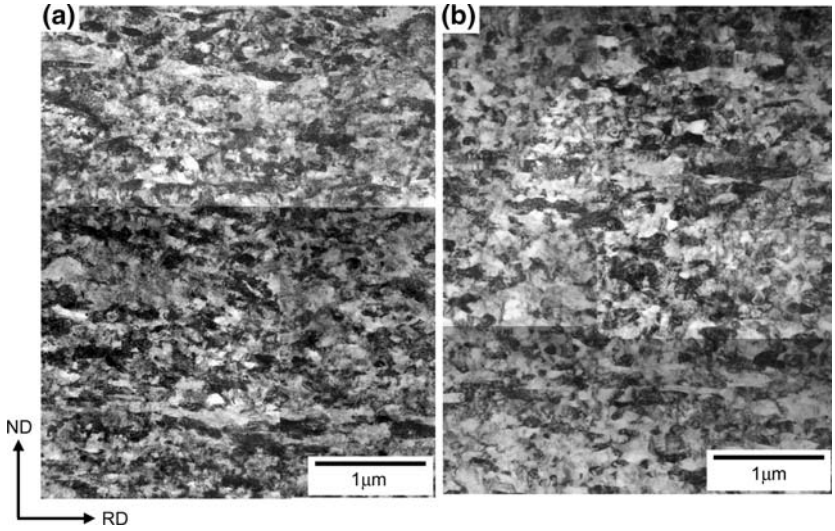

Fig. 6 TEM microstructures of the commercial purity Ti ARB-processed by (**a**) 6 cycles and (**b**) 8 cycles

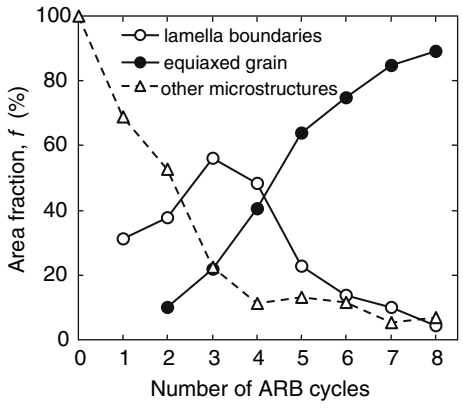

Fig. 7 Volume fraction of characteristic microstructures in the commercial purity Ti ARB-processed by various cycles at room temperature

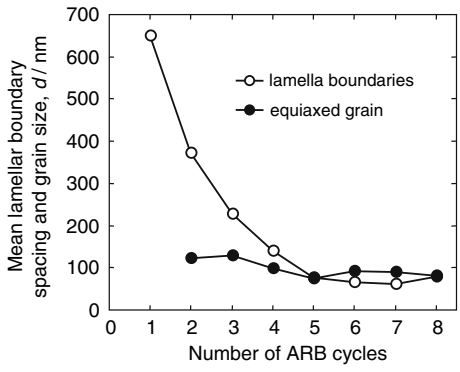

Fig. 8 Mean lamellar boundary spacing and equiaxed grain size in the commercial purity Ti ARB-processed by various cycles at room temperature

showed the maximum value of 55% at 3 cycles, and then decreased with increasing strain. On the other hand, the area fraction of the equiaxed grains monotonously increased as the ARB cycle increased, and 90% of the specimen showed the equiaxed grain structure after 8 ARB cycles. Figure 8 shows the mean lamellar boundary spacing and the mean equiaxed grain size in the CP-Ti specimens as a function of the number of ARB cycle. The values were measured on the TEM micrographs. The lamellar boundary interval significantly decreased with increasing the number of ARB cycle. On the other hand, the equiaxed grains showed very fine grain size of about 100 nm even after 2 ARB cycles. Both became nearly the same values of 80–90 nm after 5 ARB cycles.

Mechanical properties of ARB specimens

Figure 9 shows nominal stress–strain curves of the CP-Ti sheets ARB-processed by various cycles. The strength (0.2% proof stress and tensile strength) and elongation (uniform elongation and total elongation) obtained from the curves are summarized in Fig. 10 as a function of the number of ARB cycle. By 1 ARB cycle (50% rolled), flow stress greatly increased but total elongation significantly decreased from the starting material (Fig. 9). The shapes of the stress–strain curves were completely different between the starting material and the ARB-processed specimens. The stress–strain curves of the ARB samples showed peak stress at early stage of tensile test, which indicates limited uniform elongation. In Fig. 10, it can be seen that the proof stress and tensile strength increased with increasing strain up to 6 ARB cycles. The tensile strength of the 6-ARB cycle specimen was 892 MPa, which was 2.2 times higher than that of the starting sheet. On the other hand, the uniform elongation greatly decreased down to 2.6% by 1 ARB cycle, and kept nearly a constant value after that. The total elongation also significantly dropped by 1 cycle and gradually decreased with increasing the ARB cycle. In Fig. 10, typical tensile strength and total elongation of commercial Ti-6Al-4V alloy, that is known as a high strength Ti-alloy, are plotted as broken lines for comparison. It should be noted that the tensile strength and total elongation of the CP-Ti specimens ARB-processed above 5 cycles are equivalent to those of Ti-6Al-4V.

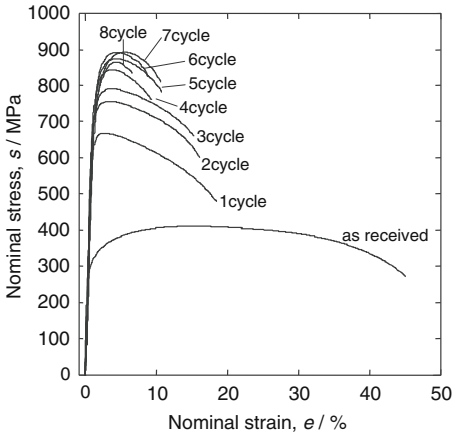

Fig. 9 Nominal stress–strain curves of the commercial purity Ti ARB-processed by various cycles at room temperature

Discussion

The change in microstructures and mechanical properties of a CP-Ti during SPD by ARB was clarified in details in the present study. It was found that two kinds of characteristic ultrafine microstructures formed in the highly deformed CP-Ti: the lamellar boundary structure and the equiaxed grains. The fraction and the dimensions of the characteristic microstructures were quantitatively clarified from the detailed microstructural observations. The equiaxed grains with grain size of about 100 nm partly appeared only after 2 ARB cycles. The fraction of the equiaxed grains monotonously increased with increasing the ARB strain, and finally 90% of the specimen was filled with the equiaxed grains after 8 ARB cycles. Such equiaxed grains have not yet been observed in the as-ARB-processed cubic metals and alloys previously studied

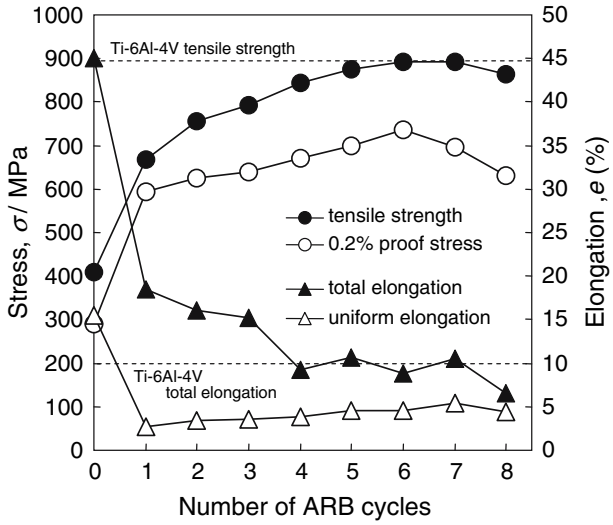

Fig. 10 Strength and elongation of the commercial purity Ti ARB-processed by various cycles at room temperature. *Broken lines* indicate typical tensile strength and total elongation of conventional Ti-6Al-4V alloy

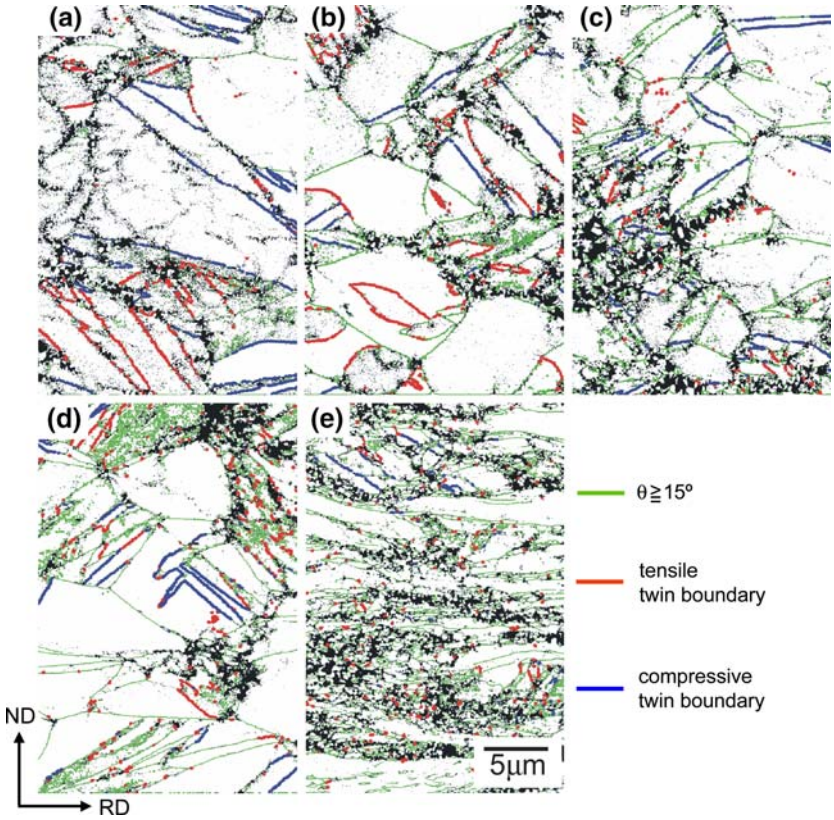

Fig. 11 Grain boundary maps obtained by EBSP measurement of the commercial purity Ti rolled to reductions in thickness of (**a**) 10%, (**b**) 20%, (**c**) 30%, (**d**) 50% and (**e**) 75% at room temperature. *Green line*, *red line* and *blue line* are high angle boundaries, tensile twin boundaries and compressive twin boundaries, respectively

[19–24]. Thus, the equiaxed grains are the characteristic feature of h.c.p. materials, or at least of h.c.p. Ti. In the materials ARB-processed previously, the equiaxed grains were observed when the ARB-processed samples were annealed [25]. However, the CP-Ti in the present study was ARB-processed at ambient temperature and no heat treatment was conducted. In this section, the mechanism of the equiaxed grains formation during the ARB process of CP-Ti is discussed.

It is well known that deformation twining plays an important role for plastic deformation in h.c.p. metals that have limited number of active slip systems. In Ti, also {1012}⟨1011⟩ tensile twin and {1122}⟨1123⟩ compressive twin were reported in the deformed samples [9, 26]. In the present data shown above, however, it was difficult to know whether deformation twining formed or not. This is because the microstructural observations were carried out by SEM and TEM without local crystallography. In order to clarify the existence of deformation twins and their role for the microstructure evolution, the specimens conventionally cold-rolled by 10, 20, 30, 50 or 75% reduction in thickness were prepared and FE-SEM/EBSP analysis was conducted for the specimens. The 50 and 75% rolling correspond to 1 and 2 ARB cycles, respectively. Figure 11 shows the boundary maps obtained from the EBSP measurement and analysis for the specimens cold-rolled by various reductions. The step size of the EBSP measurement was 50 nm. In the boundary maps, high-angle boundaries having misorientation larger than 15°, {1012}⟨1011⟩ tensile twin boundaries and {1122}⟨1123⟩ compressive twin boundaries were drawn in green, red and blue boundaries, respectively. In the 10% cold-rolled sample, both tensile and compressive twins were observed, though the deformation mode is rolling (ideally plane-strain compression). This probably depends on the orientation of each grain. The width of twins was several micrometer for both tensile and compressive twins. With increasing the total reduction, however, the fraction of twin boundaries did not significantly increased but rather decreased, while high angle boundaries (green boundaries) increased. In the 30% rolled specimen, the identical boundaries showed both blue (or red) and green colors. This indicates that the twin boundaries formed at lower reduction changed to normal high-angle boundaries owing to lattice rotation during plastic deformation. However, fresh twins no longer appeared after 50%, so that most of the boundaries observed in the 75% rolled sample were green boundaries (high-angle boundaries). This tendency is consistent with the result reported by Chun et al. [26]. In case of shearing deformation, no twins were observed in deformed area [27]. Furthermore, no micro-twins were found in the present TEM for the

ARB-processed specimens (Figs. 5, 6). These results indicated that twinning did not occur during deformation at high strain. Hence, the deformation twining has little influence on the ultrafine microstructure evolution in the specimens ARB-processed by many cycles.

Some of the shear bands in the 2 ARB cycles contained nearly equiaxed grain structures (Fig. 4d). Chichili et al. reported that the equiaxed grain structure formed by the localization of dynamic shearing deformation using the compression-torsion Kolsky bar [27]. These suggest the importance of shear banding for the equiaxed grains formation. Ti with h.c.p. crystal has less number of active slip systems than cubic materials, so that it is difficult to provide five independent slip systems in each grain which are required for von Mises criterion in polycrystalline deformation. The macroscopic shear bands probably appeared in order to accommodate the total deformation under such a situation. Within the shear bands, very large shear strain localizes, so that higher density of dislocations and finer microstructures are expected to form. Additionally, adiabatic heating is also remarkable because of strain localization. It should be noted that the thermal conductivity of Ti is especially low (17 W m^{-1} $°C^{-1}$) compared with other metals. That is, significant increase in local temperature is expected within the shear bands in CP-Ti, which assists the recovery of the regions having high density of defects to form equiaxed grain structures. It seems, therefore, reasonable that the equiaxed grains formed within the shear bands because of enhanced recovery during the process. However, the area fraction of cumulative shear bands increased to only 23% even after 8 ARB cycles (Fig. 3), while the fraction of the equiaxed grains reached to 90% in the 8-cycle ARB specimen (Fig. 7). This means that another microstructural mechanism(s) should be considered for the equiaxed grain formation in addition to the macroscopic shear bands. One of the possible mechanisms is micro shear bands that were not clearly observed in the present experiments. As was shown in Fig. 7, the fact that the fraction of the lamellar boundaries decreased while the fraction of equiaxed grains significantly increased suggests that the lamellar boundary structures turned into the equiaxed grains. It is probable that homogeneous deformation by dislocation slip is difficult in the lamellar boundary structures with intervals of 200 nm or less. The texture developed in the lamellar boundary structure may also make the dislocation slip difficult in this h.c.p. metal. Under such a situation, inhomogeneous deformation like micro shear banding might occur at the lamellar boundary region as well as macroscopic shear bonding, resulting in high density of lattice defects and local adiabatic heating that assist recovery during SPD to form the equiaxed grains. Anyhow, the high strength of the ARB-processed CP-Ti is attributed to the ultrafine microstructures with mean grain size of 80 nm.

Conclusions

The microstructure and mechanical properties of a CP-Ti severely deformed by the ARB process up to 8 ARB cycles were investigated. The main results are summarized below:

1. UFG microstructures were formed in the CP-Ti highly deformed by the ARB process.
2. Deformation twins formed at low strain below 50% rolling reduction but they disappeared at higher reduction above 75%. Therefore, deformation twining has little influence on the ultrafine microstructure evolution.
3. Two kinds of characteristic ultrafine microstructures were observed in the ARB-processed CP-Ti. One was the lamellar boundary structure elongated along RD, which has been observed in the ARB-processed materials having cubic crystal structures. The other was the equiaxed grains with mean grain size of 80–100 nm, which has not yet been found in the ARB-processed metals and alloys previously studied.
4. It was suggested that the fine equiaxed grains were formed by recovery at inhomogeneously deformed regions, such as macroscopic and micro shear bands, where very large shear strain localizes. Local adiabatic heating caused by low thermal conductivity of Ti might also assist the recovery.
5. The ARB-processed CP-Ti having the UFG microstructures showed high-performance mechanical properties equivalent to those of commercial Ti-6Al-4V alloy.

Acknowledgements The present research was financially supported by the twenty-first century COE program, the Center of Excellence for Advanced Structural and Functional Materials Design at Osaka University through the Ministry of Education, Culture, Sports, Science and Technology of Japan, and the Grant-in-Aid for Scientific Research (C), project No.17560632 in 2005.

References

1. Segal VM (1995) Mater Sci Eng A 197:157
2. Belyakov A, Kaibyshev R (1995) Nanostruct Mater 6:893

3. Iwahashi Y, Furukawa M, Horita Z, Nemoto M, Langdon TG (1998) Metall Mater Trans A 29:2245
4. Islamgaliev RK, Yunusova NF, Sabirov IN, Sergueeva AV, Valiev RZ (2001) Mater Sci Eng A 319:877
5. Tsuji N, Saito Y, Lee SH (2003) Minamino Y Adv Eng Mater 5:38
6. Huang X, Tsuji N, Hansen N, Minamino Y (2003) Mater Sci Eng A 340:265
7. Tsuji N, Kamikawa N, Ninamino Y (2004) Mater Sci Froum 467–470:341
8. Hansen N, Jensen DJ (1999) Philos Trans R Soc Lond A 357:1447
9. Yoo MH (1981) Metall Trans A 12A:409
10. Propov AA, Pyshmintsev YUI, Demakov SL, Illarionov AG, Lowe TC, Segeyeva AV, Valiev RZ (1997) Scr Mater 37:1089
11. Salishchev GA, Galeyev RM, Malysheva SP, Myshleaev MM (1999) Nanostruct Mater 11:407
12. Stolyarov VV, Zhu YT, Lowe TC, Islamgaliev RK, Valiev RZ (1999) Nanostruct Mater 11:947
13. Sergueeva AV, Stolyarov VV, Valiev RV, Mukhrjee AK (2001) Scr Mater 45:747
14. Vinogradov YUA, Stolyarv VV, Hashimoto S (2001) Valiev RZ Mater Sci Eng A 318:163
15. Stolyarov VV, Zhu YT, Alexandrov IV, Lowe TC, Valiev RZ (2003) Mater Sci Eng A 343:43
16. Stolyarov VV, Zhu YT, Raab GI, Zharikov AI, Valiev RZ (2004) Mater Sci Eng A 385:309
17. Mironov YUS, Salishchev GA, Myshlyaev MM, Pippan R (2006) Mater Sci Eng A 418:257
18. Dinda GP, Rösner H (2005) Wilde G Scr Mater 52:577
19. Saito Y, Tsuji N, Utsunomiya H, Sakai T, Hong RG (1998) Scr Mater 39:1221
20. Tsuji N, Saito Y, Utsunomiya H, Tanigawa S (1999) Scr Mater 40:795
21. Saito Y, Utsunomiya H, Tsuji N, Sakai T (1999) Acta Mater 47:579
22. Hansen N, Huang X, Ueji R, Tsuji N (2004) Mater Sci Eng A 387–389:191
23. Tsuji N, Ueji R, Minamino Y (2002) Scr Mater 47:69
24. Kamikawa N, Tsuji N, Minamino Y (2004) Sci Technol Adv Mater 5:163
25. Tsuji N, Ito Y, Saito Y, Minamino Y (2002) Scr Mater 47:893
26. Chun YB, Yu SH, Semiatin SL, Hwang SK (2005) Mater Sci Eng A 398:209
27. Chichili DR, Ramesh KT, Hemker KJ (2004) J Mech Phys Solids 52:1889